AIAA Modeling and Simulation Technologies Conference
2 - 5 August 2010, Toronto, Ontario Canada

AIAA 2010-7915

Identification of the Feedback Component of the Neuromuscular System in a Pitch Control Task

H.J. Damveld[*], D.A. Abbink[†], M. Mulder[‡], M. Mulder[§], M.M. van Paassen[¶], F.C.T. van der Helm[‖]

Delft University of Technology, Delft, The Netherlands.

and R.J.A.W. Hosman[**]

AMS Consult, Delfgauw, The Netherlands.

This goal of this study is to understand which parts of the the neuromuscular system contribute during a pitch control task. A novel method developed at the Delft University of Technology allows us to determine the contribution of the neuromuscular feedback system by identifying the admittance, which is the frequency response function of the yielded displacement due to an external force perturbation which applied to control inceptor.

In an experiment in a full-motion flight simulator, the neuromuscular admittance was identified during a longitudinal pitch tracking task with a side stick, for two different side stick configurations, an approach configuration with a relatively low stick stiffness, and a cruise configuration with a high stiffness. Besides the admittance, also the muscle activity of eleven muscles was measured. To validate whether the external force perturbation changed the control behavior of the pilot, the visual and vestibular response functions were identified as well.

From the measured results it could be concluded that the variations of the control inceptor settings had a significant effect on the neuromuscular feedback system (admittance), although the overall lumped neuromuscular system did not change significantly. A very interesting finding were the very high levels of co-contraction measured during the pitch tracking tasks. And lastly it could be concluded that the required external force perturbation did not affect the control behavior.

Nomenclature

b	Damping (Ns/rad)		
f_d	Disturbance forcing function (rad)	EMG_{rel}	Normalized electromyographic activity (-)
f_t	Target forcing function (rad)	F_{cm}	Commanded muscle force (N)
f_q	Force disturbance forcing function (N)	F_c	Contact force (N)
k	Stiffness (N/rad)	F_s	Total force acting on the stick (N)
m	Mass (Ns^2/rad)	H_{ac}	Aircraft pitch attitude
q	Aircraft pitch rate (rad/s)	H_{act}	Muscle activation dynamics
u_d	Desired control inceptor deflection (rad)	H_{adm}	Neuromuscular admittance
u_r	Realized control inceptor deflection (rad)	H_{cont}	Contact dynamics

[*] Postdoctoral Research Fellow, Faculty of Aerospace Engineering, Control and Simulation Division, H.J.Damveld@TUDelft.nl, P.O. Box 5058, 2600 GB Delft, The Netherlands.

[†] Assistant Professor, Faculty 3mE, BioMechanical Engineering, D.A.Abbink@TUDelft.nl, P.O. Box 5058, 2600 GB Delft, The Netherlands.

[‡] Researcher, Faculty of Aerospace Engineering, Control and Simulation Division, Mark.Mulder@TUDelft.nl, P.O. Box 5058, 2600 GB Delft, The Netherlands.

[§] Professor, Faculty of Aerospace Engineering, Control and Simulation Division, M.Mulder@tudelft.nl, P.O. Box 5058, 2600 GB Delft,The Netherlands.

[¶] Associate Professor, Faculty of Aerospace Engineering, Control and Simulation Division, M.M.vanPaassen@tudelft.nl, P.O. Box 5058, 2600 GB Delft,The Netherlands.

[‖] Professor, Faculty 3mE, BioMechanical Engineering, F.C.T.vanderHelm@TUDelft.nl, P.O. Box 5058, 2600 GB Delft, The Netherlands.

[**] Director, AMS Consult, R.Hosman@AMSConsult.demon.nl, Dijkgraafstraat 26, 2645 KN, Delfgauw, The Netherlands.

H_{disp}	Display dynamics	H_{nms}	Combined neuromuscular and inceptor dyn.
H_{eye}	Eye dynamics	H_{scc}	Semicircular canals
$H_{eq_{nms}}$	Neuromuscular equalization	H_{intrin}	Intrinsic stiffness of (co-)activated muscles
$H_{eq_{vis}}$	Visual equalization		
$H_{eq_{ves}}$	Vestibular equalization	θ	Aircraft pitch attitude (rad)
H_{gto}	Golgi tendon organ dynamics	ζ_{nm}	Neuromuscular damping (-)
H_{limb}	Limb inertia	τ_v	Visual process time delay (s)
H_{inc}	Control inceptor	τ_m	Vestibular process time delay (s)
H_{mf}	Motion filter dynamics	ω_{nm}	Neuromuscular frequency (rad/s)
H_{ms}	Reflexive muscle spindle feedback		

I. Introduction

The research in this paper is part of a study[1–3] to determine the adequacy of the current Obstacle Free Zones (OFZ) around runways due to the introduction of the New Large Aircraft (NLA) such as the Airbus A-380 and the Boeing 747-8. The study requires a large number of missed approaches, or balked landing maneuvers, to be performed in a monte carlo simulation. These simulations require a mathematical model of the human pilot, capable of performing a landing using the same visual, vestibular and haptic cues as a real human pilot would use. Investigations of existing pilot models[4–6] revealed that present models are rather crude and lack the level of detail required to model the interaction between the human pilot and the control inceptor, such as the control column or side-stick.

Apart from serving as an input of control commands to the aircraft, the control inceptor also serves as an input to the human pilot in terms of control forces and displacements. When a *reversible* flight control system is applied, these forces and displacements are governed by the aerodynamic forces on the control surfaces and the linkage layout. As a result, stick forces can be caused both by *planned* aerodynamic control surface forces due to deflections of the control surfaces, and by *unplanned* forces due to gusts, turbulence or buffeting.

With an *irreversible* flight control system, the control forces are generated by an artificial feel system. In this case, either the control inceptor's *position* or *applied force* can serve as the primary input. In the first case, the feel system is in series with the aircraft's flight control system and the position output of the feel system serves as input to the aircraft's flight control system. This feel system can be very elaborate, such as the *actively* loaded q-feel system applied in many aircraft (B737, B747), in which the feel force is proportional to the equivalent airspeed. On the other hand, the feel system can be very basic, such as the *passive* spring-loaded side stick present in other aircraft (A330, A340, VFW-614). Using the applied force as the primary input, the feel system is connected parallel to the flight control system. It sometimes can be very basic,[7] such as the passive rigid side stick used in some fighter aircraft (YF-16). When irreversible control systems are used, usually only the planned aerodynamic forced due to surface deflections are represented by the feel system, since generating the unplanned forces would require measuring the aerodynamic control surface hinge moments. Forces due to stall buffeting are usually taken care of by special effects, such as stick shakers, or are prevented to occur in the first place by the flight control system.

The present paper is limited to the application of irreversible flight control systems with position-based feel systems as found in almost all large transport aircraft.

The interaction with the feel system occurs through the human *neuromuscular system*, which consists of the skeleton (linkage system), muscles (actuators), proprioceptors that provide position and force feedback (a sensor system) and the central nervous system (a controller). The neuromuscular system is assumed to consist of a feedback and a feedforward component.[8] The feedforward part compensates for the dynamic properties of the human's limbs and the control inceptor. The feedback part provides the central nervous system with information about limb position and muscle forces, and can influence the response to internal noise and external force perturbations. The neuromuscular system is very adaptive and overdetermined: for instance, the stiffness of the neuromuscular system can be adjusted independently by co-contraction and by reflexive feedback activity, in order to adequately respond to external forces.

The goal of the present study is to understand which parts of the the neuromuscular system contribute during an active pitch control task. Methods,[9] developed in the Biomechanical Engineering department of the Delft University of Technology, enable us to obtain a model of the neuromuscular system from measurements. These methods have predominantly been used for postural tasks (maintaining a position or force), but have recently been extended to vehicular control tasks (car following[10] and aircraft control[11]). In this paper these methods will be applied to an aircraft pitch tracking task in the full-motion Simona Research Simulator, using an active side stick. To determine the neuromuscular system's variability, two aircraft configurations, an approach and a cruise configuration, were investigated,

using the corresponding feel system configurations proportional to the equivalent airspeed.

The novel methods are comprised of the identification of the neuromuscular *admittance*, which is the resulting amount of displacement of the control inceptor due to a force perturbation by the inceptor. In other words, the admittance is the reciproke of the stiffness. The admittance allows us to understand in general terms which parts of the neuromuscular system are involved.

To validate the identified admittance, the activity of the dominant muscles involved in generating longitudinal stick deflections was measured using electromyographic (EMG) measurements. This enables us, for instance, to determine the amount of muscle contractions, as well as co-contraction of antagonist muscle pairs (e.g., biceps and triceps). Similar studies for joystick control are known in literature,[12] but have not been applied to aircraft control.

In the remainder of this paper, first some background knowledge about the neuromuscular system's physiology and adaptability will be provided. as well as ways to model the neuromuscular system. In the following section, the methods to determine the neuromuscular admittance are explained. Subsequently the experiment setup and the results are presented. The paper concludes with a discussion of the results and conclusions.

II. Neuromuscular System

When pilots manually control an aircraft, they need to exert forces on the control column in order to realize the desired inputs to the aircraft. The neuromuscular system is responsible for realizing these forces. In most literature that describes pilot or driver behavior, the NMS is seen only as a limiting factor and modeled by a second-order low-pass filter.[5] However, the NMS also functions as a fast feedback control system (due to reflexive activity and instantaneous muscle visco-elasticity), allowing pilots to respond intuitively to side stick forces, much faster than visual or vestibular cues would allow. The need to account for such neuromuscular feedback may be small in most normal flight conditions with large aircrafts because relevant force cues may be absent (due to irreversible feel systems, or because the pilot has released the side stick). However, neuromuscular feedback becomes important when side stick forces provide the pilot with relevant feedback about aircraft states; either directly (in case of a mechanical cable/rod connections between control column and control surfaces in small aircraft) or indirectly (in case of reversible feel systems in hydraulically actuated aircraft). Another situation where neuromuscular behavior substantially influences the pilot's response is in case of biodynamic feedthrough[13] or haptic guidance systems that are currently under development.[14]

The purpose of this section is to provide the reader with some essential properties of the NMS, in order to understand the rest of the paper.

II.A. Physiology of the Neuromuscular System

The essential components of the NMS can be likened to those of a robot: a linkage (skeleton), actuators (muscles), a sensor system (proprioceptors that provide position and force feedback) and a controller (the central nervous system) which is connected to the actuators and sensors by wires (nerves). The central nervous system (CNS) consists of the brain and the spinal cord. It receives and integrates feedback from the proprioceptive sensors with relevant information from other sensors (e.g., visual, auditory and vestibular), and can send a neural command through the spinal cord to contract muscles or relax. Neural commands travel along nerves via electrochemical processes, and the traveled distance is one of the factors that influence the resultant transport time delays. Muscle activity is commanded through the alpha-motoneuron, a gathering point of neural commands from the CNS that is located in the spinal cord.

Muscles are connected to the skeleton by tendons, and can generate force only by contracting. Therefore, muscles always come in pairs so that a joint can move back and forth. An important property of muscles is that the generated force does not only depend on the activation level, but also on muscle length and stretch velocity. These so-called force-length and force-velocity relations can be simplified to effective joint stiffness and viscosity during linearized conditions. Simply put: a higher level of muscle activation does not only increase the muscle force, it also increases the muscle stiffness and viscosity. This phenomenon explains why muscle co-contraction is an effective way to stabilize a joint: although there is no change in the resulting torque around the joint, the increased activation of the muscles have caused them to become more stiff and viscous, thereby increasing the joint's instantaneous resistance to perturbations.

Another strategy to respond to external forces is through fast feedback from proprioceptive organs, that provide information about muscle force (from Golgi tendon organs), and about muscle stretch and stretch velocity (from muscles spindles). The information is sent to higher levels of the CNS, but also straight back to the alpha-motoneuron, forming a fast feedback loop. These feedback loops are called spinal reflexes. Compared to feedback from other sensors, spinal reflexes allow for substantially faster contributions to motion control than from visual or vestibular feedback. Com-

pared to muscle co-contraction, reflexive feedback is an energy-efficient way to respond to perturbations, although the inherent neural transport delays limit the frequency-bandwidth of effective response. Co-contraction and reflexive activity occur simultaneously, and it is difficult to separate their contributions to motion control. It is usually attempted by studying the electromyographical (EMG) and mechanical responses to perturbations. An informative representation of the mechanical response is the *admittance*, which is the frequency response function from force to position, or simply put the yielded displacement due to an external force perturbation. Literature shows that both mechanical and electromyographical responses depend on a variety of experimental conditions, such as task instruction,[10,15–17] the level of muscle contraction,[18] the displacement amplitude,[19,20] the frequency content of the perturbation signal[9] and the mechanical load with which the subject interacts.[21]

In other words, one of the most characteristic properties of the neuromuscular system is that it is very adaptable, allowing humans to optimally interact with their environment in a wide variety of situations.

II.B. Adaptability

The adaptability of the neuromuscular system has been demonstrated extensively in a number of studies[22–24] in which a test subject was required to perform three different tasks in face of continuous multi-sine torque perturbations on the side stick. The most simple task is a relax task, in which the subject is asked to relax and ignore the torques on the column. In a position task, the subject is asked to actively resist the torque perturbations, and keep the control column in a fixed position. During a force task, the task instruction was to actively give way to the torque perturbations thereby keeping the force on the control column constant. The methods to obtain these tests have been described previously,[22–24] and yield data with which the admittance of the spinal neuromusculoskeletal system can be estimated using closed-loop system identification.

Large differences are usually observed between the three different tasks in the low-frequency admittance ($<$ 20 rad/s). For example during a position task, the subjects were capable to increase the stiffness of their limbs by approximately a factor of 10 compared to a relax task. And during a force task the subjects could become even more compliant than when relaxed, decreasing his stiffness by a factor 10 compared to a relax task. Such a large range of adaptability has been reported in previous research on the ankle joint[23,25] and the wrist joint,[24] and has been attributed to reflexive activity and instantaneous muscle visco-elasticity from contracted muscles. Note that task instruction does not influence the admittance at high high-frequency, where the inertial properties dominate the response.

To verify the neuromuscular admittance measured during the pitch tracking tasks, all participants in the experiment were also asked to perfrom the position, relax and force tasks described above.

II.C. Modeling

In order to understand how the individual components of the neuromuscular system act together to realize relevant limb motion, it is useful to model the neuromuscular system and fit the model to the measured data in order to obtain physiologically relevant parameters.

One of the most detailed functional models available[26] is shown in Figure 1. The model can be divided in two parts, the combined physical interaction part, and the neuromuscular equalization part ($H_{eq_{nms}}$). The combined physical interaction part in its turn consists of the control inceptor dynamics (H_{inc}), and the feedback part of the neuromuscular system.

The neuromuscular feedback component enables us to respond to external (side stick) and internal (motor noise) force perturbations, but it is also involved in executing (planned) motor commands governed by the neuromuscular equalization part. The feedback system consists of muscle activation dynamics (H_{act}), limb inertia (H_{limb}), intrinsic, visco-elastic muscle dynamics (H_{intrin}), grip contact dynamics (H_{cont}), and the position and force feedback loops due to the muscle spindles (H_{ms}) and the Golgi tendon organs (H_{gto}).

Although this model provides the most detail, very accurate measurements are needed to generate the correct data to fit the model to, and a wide variety of model validation techniques are necessary to gain sufficient trust in the outcome of the parameter fit procedure. The measurement data generated during this study should allow fitting of the thirteen parameters of the neuromuscular feedback system. However, the present paper focuses primarily on the acquired neuromuscular admittance.

On the other end of the spectrum lies what this paper calls the *lumped* neuromuscular system: a simple, indirectly estimated second-order model[4–6] which lumps the neuromuscular and control inceptor systems together, and can be considered the most elementary model of the realized stick deflection u_r as the result of a desired deflection u_d:

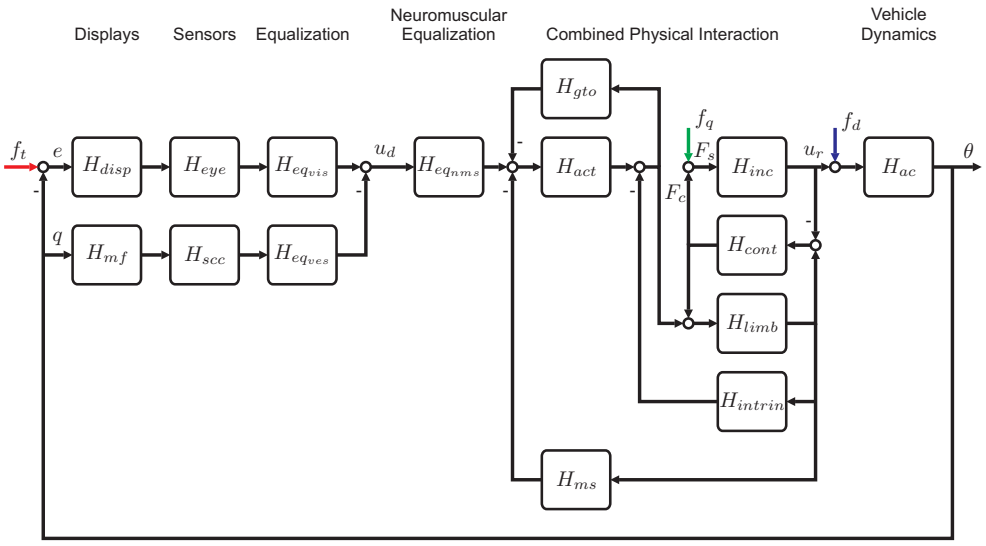

Figure 1. Pilot-aircraft pitch-tracking control loop, including a detailed physiologically based model of the neuromuscular feedforward and feedback components, taken from Ref [26].

$$H_{nms} = \frac{u_r}{u_d} = \frac{\omega_{nm}^2}{\omega_{nm}^2 + 2\zeta_{nm}\omega_{nm} j\omega + (j\omega)^2} \tag{1}$$

The second-order model is described with only two parameters: the natural frequency ω_{nm} and relative damping ζ_{nm}. Moreover, these two parameters are not fitted on measured data from side stick force or position, but instead fitted on the FRFs estimated between visual and vestibular pilot inputs and the control column position. Fig. 2 shows the lumped neuromuscular model.

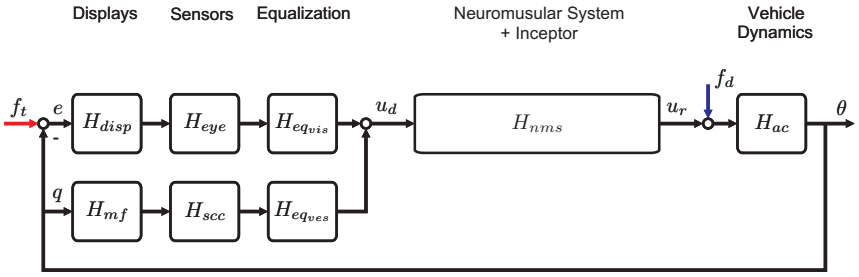

Figure 2. Pilot-aircraft pitch-tracking control loop. The neuromuscular system is modeled by a second-order low-pass filter.

III. Method

We want to investigate the effects of two control inceptor's settings on the neuromuscular system. We hypothesized, based on other studies,[27] that these effects are small, probably due to the neuromuscular feedforward part that compensates for changes in the neuromuscular's feedback component and the control inceptor. Therefore we would like to take a closer look into the separate feedforward and feedback parts. The feedforward part is located in the central nervous system (CNS) and cannot be measured directly, but the feedback part can be identified in terms of the neuromuscular admittance.

Section III.A will first describe the methods used to measure the neuromuscular admittance by introducing a very small stick force perturbation, f_q. The resulting admittance will be validated by measurements of the muscle activity of eleven of the dominant muscles governing longitudinal stick deflection, using EMG measurements.

It could be argued that the introduction of the small force perturbation might unintentionally affect the overall

control behavior To verify this, the visual and vestibular frequency response functions will be identified for both control inceptor settings, once in the presence of the force disturbance, and once without. This is described in Section III.B. Identifying the visual and vestibular frequency response functions requires the addition of two more forcing functions, f_t and f_d. The identification of the visual and vestibular frequency response functions also enables us to fit a second-order low-pass model to the lumped neuromuscular system. Also the muscle activity will be recorded with and without the force perturbations. It is assumed that the effect of the force perturbations is small if the overall control behavior and EMG activity does not change.

III.A. Neuromuscular Response

As depicted in Figure 1 in Section II, the neuromuscular system is comprised of a feedback and a feedforward component. The feedback part responds to internal and external force perturbations. The feedforward part compensates for the dynamic properties of the human's limbs and the control inceptor. This means that a change in control inceptor dynamics will be equalized by the feedforward component, and the resulting lumped neuromuscular system will hardly show any changes. The feedforward part of the neuromuscular system is located in the parietal and motor cortices[8] and cannot be measured or identified directly during pitch control. However, is is possible to identify the feedback part of the neuromuscular system, which provides feedback to the central nervous system about limb position and muscle forces, in order to adequately respond to internal noise and external force perturbations.

III.A.1. Estimating Admittance

Measuring the neuromuscular system dynamics can be achieved by introducing a third forcing function, f_q, which perturbs the contact force felt by the pilot. Three classical tasks[10] form the boundaries within which a subject can adapt the response to forces: one could choose to resist them (maintain position, or position task PT), to ignore them (relax task RT) or to actively give way (maintain constant force, or force task FT). When the force perturbation is designed correctly,[25,28] according to the Reduced Power Method, power can be low, and the subjects task-related behavior is not influenced while the neuromuscular system can be identified over a large bandwidth. This technique has also been applied during vehicular control.[10] After the experimental data has been gathered, closed-loop system identification techniques can be used to estimate the neuromuscular feedback response as the causal dynamic relationship between the measured stick force F_c (input) and stick deflections u_r (output), i.e., the admittance. It is estimated for each condition over the time-average over all repetitions, according to:

$$\hat{H}_{adm} = \hat{H}_{F_c u_r} = \frac{\hat{S}_{f_q u_r}}{\hat{S}_{f_q F_c}}. \tag{2}$$

The term $\hat{S}_{f_q u_r}$ is the estimate for the cross-spectral density of disturbance f_q and u_r, whereas $\hat{S}_{f_q F_c}$ is the cross-spectral density of disturbance f_q and F_c. All spectral densities were averaged over two adjacent frequencies to reduce the variance.

The coherence squared function was used to determine the approximation involved by using linear models. It is an indication of the amount of linearity of the system in response to the external perturbation. For a linear system, the coherence function equals one when there is no noise (linearization or measurement noise), and zero in the worst case. Generally, high coherence-squared values were found for all tasks, although somewhat lower during pitch tracking than during classical tasks.

III.A.2. Electromyographic Response

In order to provide additional measurements from inside the neuromuscular system, electromyographic (EMG) measurements were performed on eleven muscles that are expected to contribute to pitch control. Due to technical problems with the EMG measurement device during the period available for experiments, only six pilots (subjects 1,2,3,4,9 and 10) out of ten could be measured. The eleven relevant muscles are listed below, and the locations of the EMG electrodes are shown in Figure III.A.2.

The muscle activity of upper body muscles relevant to side-stick pitch control was measured with a 16-channel Bagnoli Delsys System, making use of single-differential electrodes with 10 mm interspacing. All EMG electrodes were placed and oriented according SENIAM standards. Skin conduction was improved by using local shaving of the skin, abrasion with sandpaper and cleaning with alcohol. The EMG recording system processed the EMG signals as follows. All signals were a) pre-amplified (by a factor of 100, 1000, or 10.000 per channel, which was selected

Table 1. Selected muscles: names, abbreviations, body location and main functions during pitch control.

Muscle	Abbreviation	Location	Main function
Flexor carpi radialis	FC	lower arm	grip, roll left
Extensor carpi radialis	EC	lower arm	grip, roll right
Extensor carpi ulnaris	RU	lower arm	grip, push
Extensor policis brevis	PB	lower arm	grip, pull
Triceps lateralis	TB	upper arm	push
Biceps brachii	BB	upper arm	pull
Deltoid anterior	DA	shoulder	push
Deltoid posterior	DP	shoulder	pull
Pectoralis major	PM	torso	push
Latissimus dorsi	LD	torso	pull
Trapezius	TR	neck	shoulder elevation

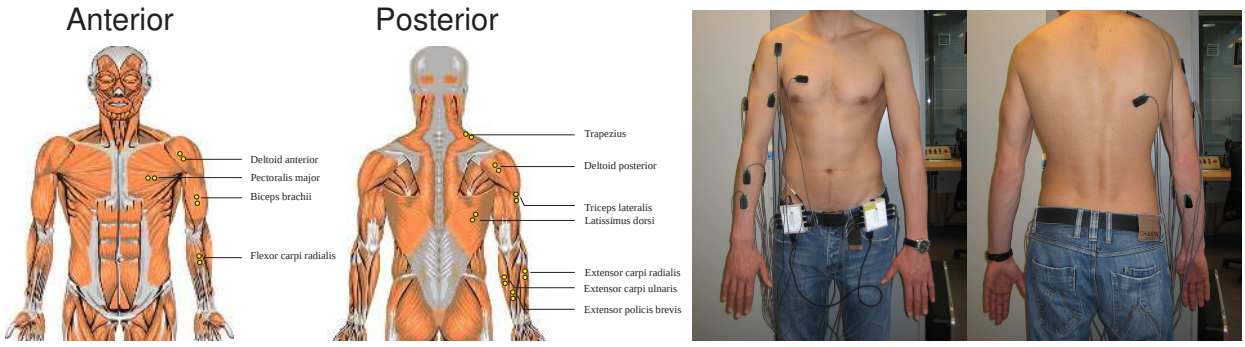

a) Schematic overview of muscle locations. **b) Typical subject showing the location of the eleven EMG electrodes.**

Figure 3. Locations of relevant muscles and electrodes for EMG measurements.

manually) to ensure the best signal-to-noise ratio; subsequently b) band-pass filtered to prevent motion artifacts and aliasing (analog 80 dB/decade, allowing only signal power between 20-450 Hz; and finally c) sampled at 1000 Hz and subsequently digitally stored on a separate laptop for further analysis. Each recorded trial was triggered by the experiment control interface of the Simona Research Simulator, ensuring synchronization between recorded EMG signals and other measured signals. Before rectifying the stored signals, they were post-processed to improve the signal-to-noise ratio: anti-causal notch-filters (width: 1 Hz) were applied around the frequency of the local powergrid (in the Netherlands: 50 Hz) plus all higher harmonics. This filtering of higher frequencies substantially improved the signal-to-noise ratio at lower frequencies after rectifying. Subsequently, the signals were rectified, filtered at 20 Hz for visualization purposes, and resampled at 100 Hz. Note, that in this paper the EMG signals are shown by normalized signals EMG_{rel}, which are calculated by dividing the absolute EMG signal by the maximal EMG signal during an isometric pushing or pulling task (with target forces 50, 100 or 200 N, or relaxing). These isometric measurements are shown in Figure 4.

III.B. Visual and Vestibular Response

In the previous section, two models of the neuromuscular system have been presented. These models were based on the assumption that the neuromuscular system attempts to realize a desired stick deflection. The input of the neuromuscular system, the desired deflection u_d, is the combined output of the visual and vestibular system. The visual system governs the pilot's response to a visual tracking error, while the vestibular system provides the response to an (angular) motion cue. It is assumed that the visual and vestibular response compensate for the vehicle dynamics in such a way that the open-loop pilot-vehicle frequency response function has integrator-like dynamics.[5] This visual and vestibular adaptation of the pilot to the vehicle dynamics is called *equalization*.

Previous studies[4,29–31] demonstrated system identification techniques[32,33] to obtain the frequency response func-

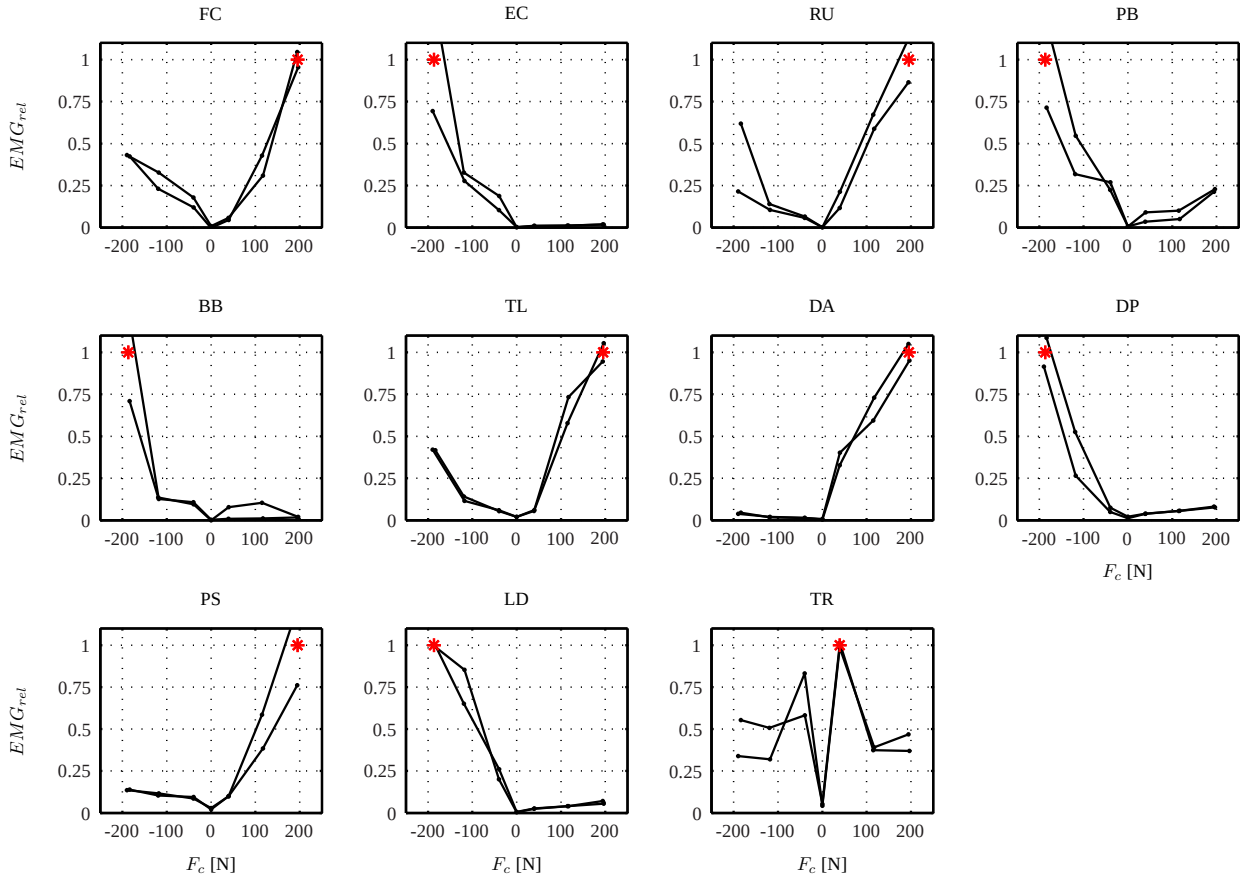

Figure 4. EMG activity of eleven muscles, during two identical isometric force tasks. The EMG measurements are normalized to the maximal EMG value averaged over the two repetitions, shown by the red star. Muscle name abbreviations are listed in Table 1. Note that pushing forces are defined as positive.

tions (FRF) of the visual system and the vestibular system in a pitch tracking task. To identify the two parallel systems, two forcing functions are required to perturb the systems distinctively. A *target* forcing function signal (f_t) is used as a commanded pitch attitude reference on a primary flight display (PFD), which the pilot is demanded to track. A *disturbance* forcing function perturbs the aircraft's elevator, and generates a pitch attitude disturbance similar to a turbulence field.

Using these two forcing functions it is possible to indirectly determine the lumped neuromuscular system by *modeling* it as a second-order low-pass filter consisting of two parameters, a natural frequency ω_{nm} and damping ratio ζ_{nm}. These parameters are then fitted, together with visual and vestibular models, to the measured visual and vestibular frequency response functions. This lumped model contains the contributions of both the neuromuscular feedforward, or equalization, component, and the feedback response.

The frequency response functions of the control inceptor displacement u to the visual error e, H_{p_e}, and to the pitch attitude θ, H_{p_θ} are defined as:

$$H_{p_e}(j\omega) = \frac{\mathrm{d}u}{\mathrm{d}e}(j\omega) = H_{disp}(j\omega)H_{eye}(j\omega)H_{eq_{vis}}(j\omega)H_{nms}(j\omega) \tag{3}$$

$$H_{p_\theta}(j\omega) = \frac{\mathrm{d}u}{\mathrm{d}\theta}(j\omega) = (j\omega)^2 H_{mf}(j\omega)H_{scc}(j\omega)H_{eq_{ves}}(j\omega)H_{nms}(j\omega) \tag{4}$$

To parameterize the identified frequency response functions, a model structure needs to be assigned to each of the components in Eqs 3 and 4. In absence of a better model, the display and eye dynamics are assumed to be simple gains: $H_{disp}(j\omega) = H_{eye}(j\omega) = 1$. In addition, the effect of the motion filters is assumed to be negligible: $H_{mf} = 1$. Based on the work by McRuer[5] the visual equalization is modeled by a gain, a lead-lag filter and a time delay:

$$H_{eq_{vis}}(j\omega) = K_v \frac{1 + j\omega T_{lead}}{1 + j\omega T_{lag}} e^{-j\omega\tau_v} \tag{5}$$

while the lumped neuromuscular system is modeled as a low pass filter:

$$H_{nms}(j\omega) = \frac{\omega_{nm}^2}{\omega_{nm}^2 + 2\zeta_{nm}\omega_{nm}j\omega + (j\omega)^2} \tag{6}$$

The vestibular equalization system is modeled by a gain and a time delay:

$$H_{eq_{ves}}(j\omega) = K_m e^{-j\omega\tau_m} \tag{7}$$

The model of the semicircular canals is given by:

$$H_{scc}(j\omega) = \frac{1 + j\omega T_{scc_1}}{1 + j\omega T_{scc_2}} \tag{8}$$

where $T_{scc_1} = 0.1s$ and $T_{scc_2} = 6.0s$ are constants taken from Ref [4].

The resulting Eqs 3 and 4 are defined by eight parameters: K_v, T_{lead}, T_{lag}, τ_v, K_m, τ_m, ω_{nm} and ζ_{nm}. These parameters are estimated by fitting the parameterized models to the identified frequency response functions.

IV. Experiment

IV.A. Hypothesis

The present study attempts to confirm the following hypotheses:

1. The variations of the control inceptor settings will have a significant effect on the neuromuscular admittance (based on findings in Refs [10, 20]).
2. Pitch tracking tasks will not require significant amounts of co-contraction (based on findings in Ref [8]).
3. The variations of the control inceptor settings will have no significant effect on the lumped neuromuscular parameters, the break frequency ω_{nm} and the damping ratio ζ_{nm} (based on findings in Ref [27]).
4. The applied force disturbance forcing function will not significantly affect the visual and vestibular control behavior, nor muscle activity, exerted during the pitch tracking task.

IV.B. Participants

Ten subjects participated in the experiment, nine males and one female. All pilots were in posession of a valid commercial pilot license (CPL) or an airline transport pilot license (ATPL) and had at least (simulator) experience with commercial passenger jet aircraft (Table 2).

Table 2. Participants and experience.

Pilot	Gender	Age	Experience
1	male	40	CPL, ATPL, A330
2	male	22	CPL, MEP, IR
3	male	22	CPL, MEP, IR
4	male	25	CPL, ATPL, B777, F100
5	male	35	CPL, ATPL, MD11, P3C
6	male	24	CPL, ATPL, F100, 900h
7	female	23	CPL, ATPL, C560XLS, 800h
8	male	65	CPL, ATPL, 16000h
9	male	34	CPL, C550
10	male	38	CPL, C550

IV.C. Task

The pilot is requested to track the pitch attitude commanded by the flight director (FD) symbol on his primary flight display (PFD, see Figure 5) as accurately as possible with the aircraft reference symbol, and consequently keep the error close to zero.

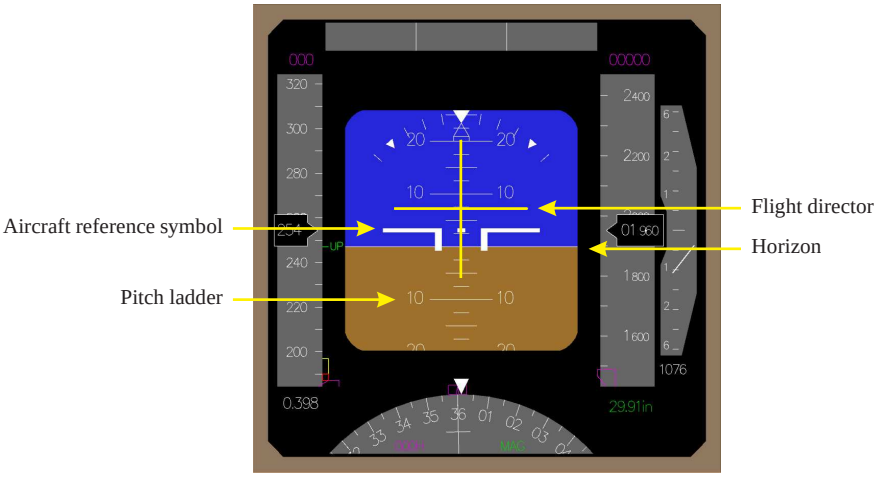

Figure 5. Primary Flight Display (PFD).

The FD shows attitude corresponding to the trimmed condition, and is directly driven by the target forcing function f_t. Since the aircraft elevator is driven by the disturbance forcing function f_d and results in a perturbed pitch attitude, the total error is the sum of th perturbed pitch attitude and the FD perturbation.

The PFD is a pursuit display type and enables the pilot to perceive the error between the FD and aircraft reference symbol, as well as the actual pitch attitude. As a result, the pilot might anticipate the movement of the target forcing function.

IV.D. Independent Variables

In the design of experiments, independent variables are those variables that are hypothesized to have an effect on the dependent measures. In the present experiment the only independent variable is the feel system setting of the side stick pitch channel.

Two sets of parameters of the feel system were chosen, a configuration with a low stiffness representing a low-speed approach setting, and a setting with a high stiffness representing cruise. The specified parameters are listen in Table 3. The actual parameters have been identified from frequency sweeps measuring the applied force to the side stick, and the corresponding deflection. These parameters are listed in Table 3 as well. Bode plots of the frequency response functions are shown in Figure 6.

Table 3. Specified and identified parameters of the longitudinal side stick dynamics.

		Approach		Cruise	
		Specified	Fitted	Specified	Fitted
m	(Ns^2/rad)	0.18	0.12	0.18	0.12
b	(Ns/rad)	4.05	3.33	4.05	5.37
k	(N/rad)	343.77	240.81	687.55	476.10

IV.E. Dependent Measures

A number of parameters were recorded during the experiment, which included the aircraft pitch attitude θ, the visual error e, the stick deflection u and the applied stick force F_e. This allowed us to calculate a number of dependent measures:

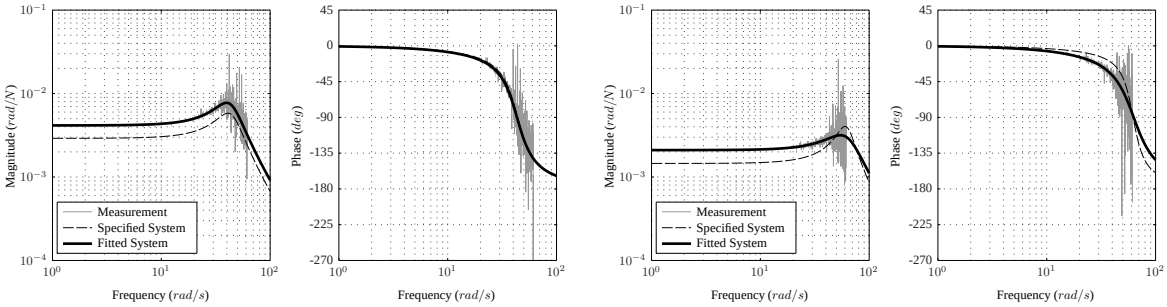

Figure 6. Bode plot of the specified and identified longitudinal side stick dynamics.

- the neuromuscular admittance frequency response function H_{adm}
- the visual frequency response function H_{vis}
- the vestibular frequency response function H_{vest}

The last three frequency response functions are used for fitting models of the visual, vestibular and neuromuscular systems. The fitted model parameters include: K_v, T_{lead}, T_lag, τ_v, K_m, τ_m, ω_{nm} and ζ_{nm}.

In order to validate the identified neuromuscular model, electromyographic (EMG) measurements were performed on eleven muscles, and the mean and standard deviation of the EMG_{rel} were determined.

IV.F. Apparatus

IV.F.1. Simona Research Simulator

The Simona research simulator (SRS), developed and built by the Delft University of Technology, was used to perform all experiments. The exterior of the SRS is shown in Figure 7a. Cabin accelerations can be generated in all 6 degrees of freedom by means of a hydraulic hexapod actuator system.

The cabin design is unconventional, consisting of a monocoque positioned directly between the actuator gimbal points. The result is a light-weight construction, capable of generating high-frequency accelerations. The collimated panoramic outside visual mirror has been attached directly to the cabin and covers a total field of view of $180°$ H $\times$ $40°$ V.

The SRS flight deck (Figure 7b) consists of a dual configuration: The captain's position contains a conventional hydraulic control column and pedals configuration, while the first officer's position is equipped with a control loaded active electric side-stick and hydraulic pedals. In the present experiment only the hydraulic control column was used.

All components of the SRS are driven by regular personal computers with various operating systems, linked together by a SCRAMNET shared-memory network. The distributed simulation and timing is taken care of by the DUECA[34] software environment. The main simulation runs at 100 Hz, including the generation of the forcing function and the data logging. The motion system and control inceptor are driven at a combination of 1 kHz and 5 kHz.

IV.F.2. EMG Measurement System

A 16 channel DelSYS Bagnoli Desktop EMG Measurement System was used to perform EMG measurements. The data was sampled at 1000 Hz by a National Instruments AD convertor.

IV.G. Control Variables

Control variables are those variables that are not changed throughout an experiment because their effect on the results is not the primary interest of that particular experiment. However, the settings of those variables can still have a significant influence on the outcome, and these variables should be selected within a suitable range. As such, the settings of these control variables should be chosen with care. The control variables in the current experiment comprise the aircraft dynamics, the motion-cueing algorithm settings, and the applied forcing functions.

a) SRS exterior. **b) SRS flight deck with the hydraulic control column.**

Figure 7. Simona Research Simulator (SRS).

IV.G.1. Aircraft Dynamics

In order to represent a New Large Aircraft, a Boeing B747-100/200 model was used.[35] The aircraft dynamics are comprised of a non-linear Flight Control System (FCS) and a non-linear aircraft model. The inputs of the FCS contained the control inceptor inputs and a number of measured aircraft states. The FCS controlled the actual aircraft elevator, flap and aileron actuators. After addition of measurement noise, the resulting aircraft states were fed back to the FCS.

In order to identify the visual and vestibular systems, the elevator of the aircraft model needs to be deflected to generate a commanded pitch attitude perturbation. Due to the nonlinearities in both the FCS and the aircraft model, addition of a disturbance to either the control inceptor deflection or directly to the elevator deflection commanded by the FCS will not always result in exactly the same attitude perturbation, and the perturbation would become dependant on the control inceptor deflection realization. As a solution, it was decided to linearize the combined FCS and aircraft dynamics.

Two trim conditions were chosen for linearization. The first condition represents the approach condition at 1500 ft and 125 kts indicated airspeed. This flight condition is representative for the first segment of the balked landing maneuver, although the flight path was chosen to be horizontal instead of at three-degree descending slope. The second is a cruise condition at 35,000 ft and 493 kts. These conditions are listed in Table 4.

Table 4. Stationary flight condition

		Approach	Cruise	
Mass	m	$190,508.6$	$190,508.6$	kg
True airspeed	V_{TAS}	64.3	253.6	m/s
Pitch attitude	θ	5.35	0.26	deg
Angle of attack	α	5.35	0.26	deg
Altitude	h	457.2	$10,668.0$	m
Vertical speed	w	0.0	0.0	m/s
Flaps	δ_{flap}	30.0	0.0	deg
Gear	δ_{gear}	down	up	
Stabilizer trim	δ_{stab}	9.0	3.6	deg

The corresponding linearized frequency response functions of the pitch attitude to a side stick deflection are shown in Figure 8.

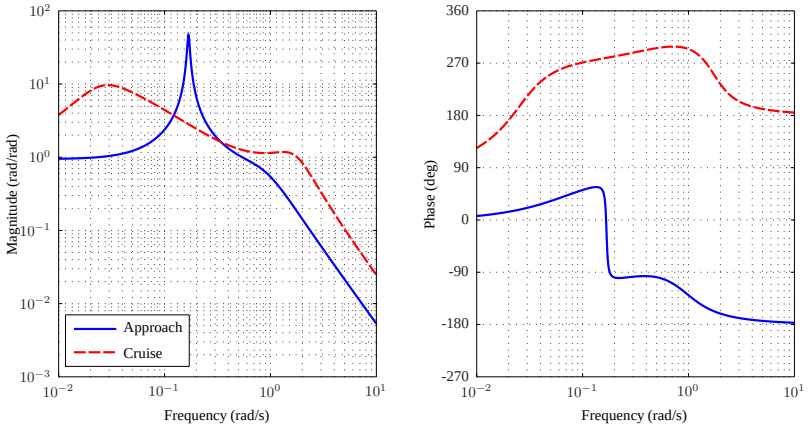

Figure 8. Frequency response of the pitch attitude due to control column deflection.

IV.G.2. Motion Filter Settings

To fit the actual aircraft motion within the motion space of the SIMONA Research Simulator, a classical linear washout motion cueing algorithm[36,37] was used. This algorithm consists of scaling and filtering the specific forces and angular accelerations. In the present experiment, no low-pass filtering or tilt-coordination was used since the tasks did not require sustained forward or lateral accelerations. Hence only high-pass filtering and scaling was applied.

A first order filter was applied to the pitch accelerations to prevent sustained pitch angles from resulting in specific force errors. A second order filter was used in the surge direction, while a third order was applied in heave direction:

$$HP_\theta(j\omega) = \frac{j\omega}{j\omega + \omega_{hp_\theta}} \tag{9}$$

$$HP_x(j\omega) = \frac{(j\omega)^2}{(j\omega)^2 + 2\zeta_{hp_x}\omega_{hp_x}j\omega + \omega_{hp_x}^2} \tag{10}$$

$$HP_z(j\omega) = \frac{(j\omega)^2}{(j\omega)^2 + 2\zeta_{hp_z}\omega_{hp_z}j\omega + \omega_{hp_z}^2} \cdot \frac{j\omega}{j\omega + \omega_{b_z}} \tag{11}$$

These filters contain six parameters (ω_{hp_θ}, ω_{hp_x}, ζ_{hp_x}, ω_{hp_z}, ζ_{hp_z} and ω_{b_z}). In combination with the three scaling gains (k_{f_x}, k_{f_z} and k_{ω_θ}), nine parameters need to be selected in total.

Since the pitch acceleration is considered the most important cue, and since the SRS is capable of simulating the pitch motion without scaling, k_{ω_θ} was selected to be 1.0, while the break-frequency ω_{hp_θ} was chosen to be 0.1 rad/s, which provides some washout to eliminate sustained false cues in surge. Figure 9a shows the resulting motion fidelity of the pitch motion according to the Sinacori criterion.[38]

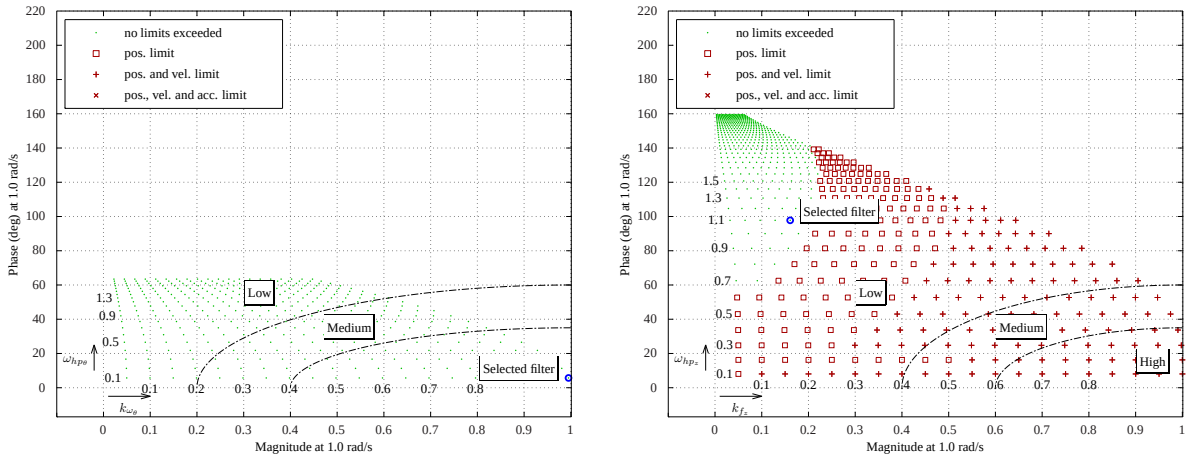

a) Pitch. **b) Heave.**

Figure 9. Motion fidelity as a function of phase distortion and gain at 1 rad/s due to high-pass washout filtering. Plotted are the boundaries proposed by Schroeder.[39]

In accordance with Ref [37], the break-frequency ω_{b_z} of the high-pass heave filter was set to 0.2 rad/s and the damping ζ_{hp_z} to 0.7. The remaining parameters, k_{f_z} and ω_{hp_z}, were selected based on Figure 9b. This figure shows the phase distortion and gain attenuation at 1 rad/s as a function of k_{f_z} and ω_{hp_z}, as well as whether the simulator motion space would be exceeded or not.

The high-pass surge filter parameters were chosen rather arbitrarily since no surge accelerations were simulated. The filter's only purpose was to eliminate false surge cues due to pitch accelerations. A summary of all motion filter parameters is given in Table 5.

Table 5. Classical linear washout motion filter settings.

High-pass surge		
k_{f_x}	0.3	-
ω_{hp_x}	2.0	rad/s
ζ_{hp_x}	0.7	-

High-pass heave		
k_{f_z}	0.25	-
ω_{hp_z}	1.1	rad/s
ζ_{hp_z}	0.7	-
ωb_z	0.2	rad/s

High-pass pitch		
k_{ω_θ}	1.0	-
ω_{hp_θ}	0.1	rad/s

IV.G.3. Forcing Functions

The three forcing functions must meet specific requirement, both from a system identification and a task requirement point of view.[40] To enable the instrumental variable system identification method, multi-sines with power at a selected number of frequencies were adopted:

$$f(t) = \sum_{j=1}^{N} A_j \sin(\omega_j t + \phi_j) \tag{12}$$

All forcing functions lasted 81.92 seconds, corresponding to a base frequency of 0.0767 rad/s. the frequencies of the sines in the multi-sines all consisted of a multiple k of the base frequence.

The power spectrum of the target forcing function f_t contains a significant amount of power at the lower frequencies to represent a realistic tracking task. In addition, a low-power high-frequency shelf was added to enable identification of the high-frequency control behavior. The total power of the target forcing function was 1.6 deg^2.

The disturbance forcing function f_d consists of sines at frequencies next to those of the target forcing function for system identification requirements. The disturbance forcing function perturbs the elevator deflection and results indirectly in a pitch attitude perturbation. It is desired that the pitch attitude power spectrum has a similar shape as the target forcing function. This is achieved by premultiplying the desired pitch attitude power spectrum by the inverse of

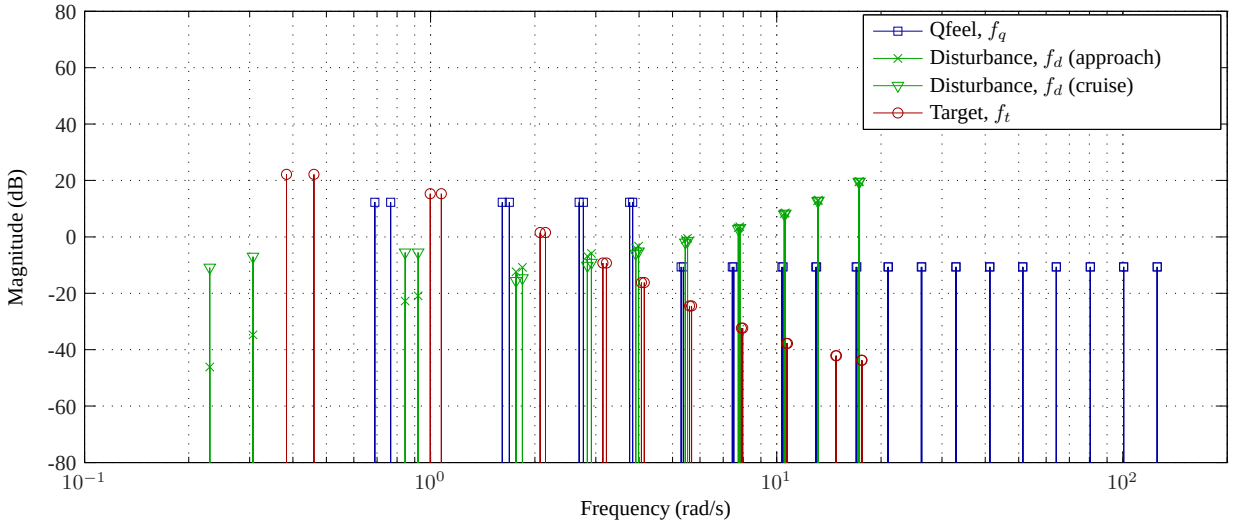

Figure 10. Power density spectra of the target, disturbance and q-feel forcing functions. The PSD's are normalized to a power of 1.0.

Table 6. Frequencies, amplitudes and phases defining the q-feel, disturbance and tracking forcing function.

Q-feel f_q				*Disturbance f_d (approach)*				*Disturbance f_d (cruise)*				*Target f_t*			
k	ω	A	ϕ	k	ω	A	ϕ	k	ω	A	ϕ	k	ω	A	ϕ
(-)	(rad/s)	(N)	(rad)	(-)	(rad/s)	(rad)	(rad)	(-)	(rad/s)	(rad)	(rad)	(-)	(rad/s)	(rad)	(rad)
9	0.690	0.447	2.858	3	0.230	0.016	−1.531	3	0.230	0.118	3.158	5	0.383	0.792	−1.558
10	0.767	0.447	0.659	4	0.307	0.030	−0.809	4	0.307	0.147	−0.979	6	0.460	0.792	4.210
21	1.611	0.447	4.279	11	0.844	0.060	0.375	11	0.844	0.161	3.415	13	0.997	0.534	0.966
22	1.687	0.447	3.949	12	0.920	0.066	2.480	12	0.920	0.161	3.358	14	1.074	0.534	−0.395
35	2.684	0.447	0.673	23	1.764	0.108	1.551	23	1.764	0.090	−1.304	27	2.071	0.241	4.241
36	2.761	0.447	1.587	24	1.841	0.118	1.168	24	1.841	0.095	0.243	28	2.148	0.241	0.885
49	3.758	0.447	0.083	37	2.838	0.149	−1.305	37	2.838	0.123	4.041	41	3.145	0.130	2.102
50	3.835	0.447	2.183	38	2.915	0.157	−1.235	38	2.915	0.131	0.390	42	3.221	0.130	−0.248
69	5.292	0.120	−0.925	51	3.912	0.176	3.273	51	3.912	0.157	0.182	53	4.065	0.087	−0.225
70	5.369	0.120	0.820	52	3.988	0.183	3.596	52	3.988	0.164	−1.133	54	4.142	0.087	−1.015
97	7.440	0.120	−0.318	71	5.446	0.209	−1.502	71	5.446	0.197	2.844	73	5.599	0.054	4.212
98	7.517	0.120	2.299	72	5.522	0.215	2.637	72	5.522	0.203	2.665	74	5.676	0.054	1.808
135	10.354	0.120	4.100	101	7.747	0.266	4.247	101	7.747	0.259	3.261	103	7.900	0.034	−1.329
136	10.431	0.120	2.874	102	7.823	0.272	1.304	102	7.823	0.264	1.796	104	7.977	0.034	2.065
169	12.962	0.120	0.784	137	10.508	0.355	0.440	137	10.508	0.350	−1.163	139	10.661	0.025	−1.498
170	13.039	0.120	−0.753	138	10.584	0.360	2.065	138	10.584	0.355	0.432	140	10.738	0.025	−0.622
221	16.950	0.120	3.814	171	13.116	0.462	2.085	171	13.116	0.458	1.997	193	14.803	0.020	1.703
222	17.027	0.120	1.407	172	13.192	0.468	1.997	172	13.192	0.463	0.075	194	14.880	0.020	3.069
273	20.939	0.120	3.183	225	17.257	0.679	1.550	225	17.257	0.676	−1.060	229	17.564	0.018	−1.091
274	21.016	0.120	0.470	226	17.334	0.685	−1.292	226	17.334	0.682	4.497	230	17.641	0.018	−0.053
341	26.154	0.120	1.093												
342	26.231	0.120	−0.811												
429	32.904	0.120	1.324												
430	32.981	0.120	2.105												
537	41.187	0.120	−1.240												
538	41.264	0.120	−0.942												
669	51.312	0.120	0.544												
670	51.388	0.120	2.237												
837	64.197	0.120	3.156												
838	64.274	0.120	−0.967												
1049	80.457	0.120	−0.836												
1050	80.534	0.120	−1.414												
1309	100.399	0.120	−1.184												
1310	100.476	0.120	3.920												
1637	125.556	0.120	2.483												
1638	125.633	0.120	3.519												

the linearized aircraft and FCS dynamics. The power of the pitch attitude disturbance was set to 1.6 deg^2. This results in a power of f_d of 297.7 deg^2 for the approach configuration and a power of 14.3 deg^2 for the cruise configuration.

The q-feel forcing function f_q is comprised of a high-power low-frequency part and a low-power high-frequency shelf according to the reduced power method.[28,41] To reduce the unwanted effects on the neuromuscular system due to the presence of control inceptor force perturbation, the power of the q-feel forcing function was selected as low as possible while still enabling adequate coherence values. The power of the q-feel forcing function amounted to 1.0 $(\mathrm{N})^2$.

The power density spectra of the target, disturbance and q-feel forcing functions are displayed in Figure 10. Table 6 lists the base-frequency multiple k, the actual frequency ω, the amplitude A and the phase ϕ of each of the sines in the forcing functions.

V. Results

V.A. Admittance

Figure 11 shows the neuromuscular admittance measured during a position, relax and force task, as well as during the approach and cruise conditions of the pitch tracking task. The admittance is averaged over all the participants, the errorbars show the standard deviation. At high frequencies, the admittance is small for all tasks: inertial properties dominate the response to forces. Figure 11a illustrates that at low frequencies, all subjects showed a large range of adaptability for different classical task: during position tasks the admittance is smaller than during relax tasks, while during FT the admittance is even larger than when relaxed.

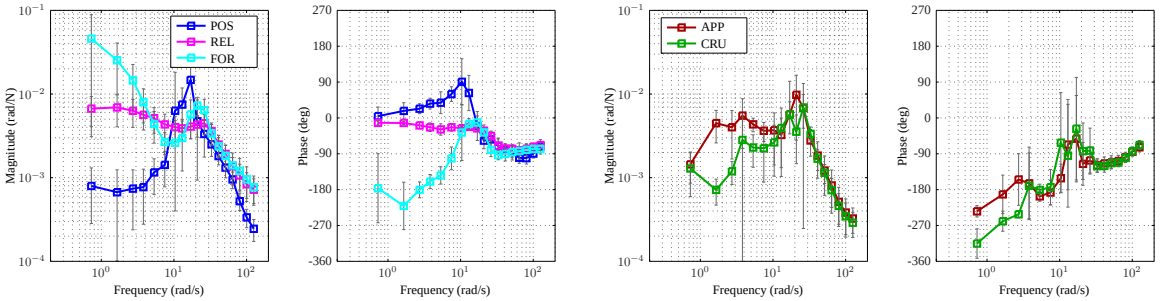

a) Position, relax and force tasks. **b) Approach and cruise pitch tracking tasks.**

c) Position, relax and force tasks, approach and cruise pitch tracking tasks.

Figure 11. Neuromuscular admittance frequency response functions.

Figure 11b shows that the admittance during cruise conditions (CRU) is lower than during approach conditions (APP) below 20 rad/s, suggesting that during cruise conditions there is either more co-contraction, more reflexive activity or more passive visco-elasticity (due to smaller stick deviation amplitudes). Comparing the pitch control conditions to the classical tasks (Figure 11c) shows that the admittances of both conditions of pitch tracking lie between the position and relax task. In other words, the neuromuscular system is more stiff than when relaxed, indicating some co-contraction and/or reflexive activity. The peak around 20 rad/s suggests that some reflexive activity is present. Another interesting comparison is that the admittance beyond 50 rad/s is smallest during position tasks and pitch control tasks, more closely resembling a second-order decay. This indicates a very stiff coupling between limb inertia

and stick inertia. In other words, during pitch tracking, the grip is as stiff as during a position task. During relax and force tasks, subjects tend not to grip the stick so strongly.

V.B. Muscle Activity

The EMG_rel was repeatable within the six subjects from whom EMG measurements were obtained, but some inter-subject variability was present. In order to provide an easily interpretable overview of the measured muscle activity, the EMG_{rel} of the eight most important muscles was characterized by the mean (a measure of steady contraction) and the standard deviation (a measure of variation around the mean contraction). Figure Figure 12 shows the mean of EMG_{rel}, for all six pilots, and for all conditions.

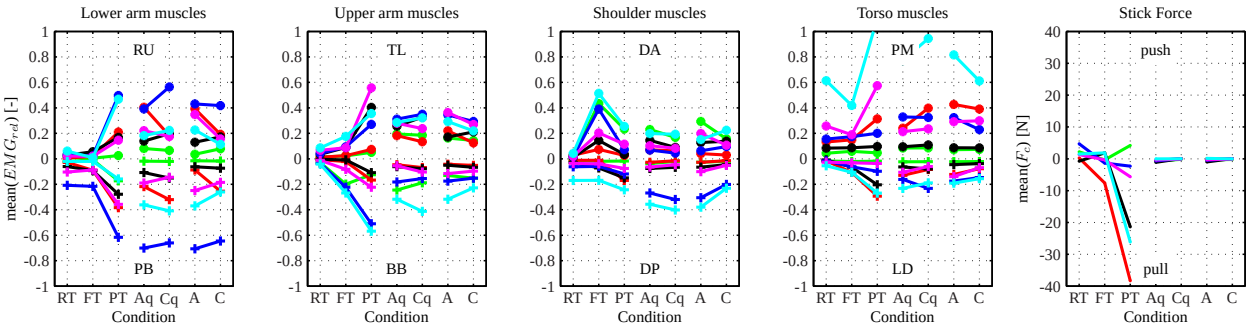

Figure 12. Mean of the relative muscle activity EMG_{rel} for eight muscles of six pilots (1,2,3,4,9,10), measured over three runs. The top panels show muscles that are mainly active during pushing the stick, the bottom panels muscles that are mainly active during pulling.

As can be expected, for all muscles the activity is negligible during the relax task RT. When trying to maximally resist the forces (during position task PT), both pulling and pushing muscles are active at around 30-60$\%$ of the maximal activity (levels of activation common during a PT[10]). The co-contraction is useful to resist perturbations, but costs substantial amounts of metabolic energy. During all pitch tracking conditions similar levels of co-contraction are observed. Co-contraction levels are similar between approach and cruise conditions, both in presence of force perturbations f_q(conditions A_q and C_q) or when these are absent (conditions A and C). Note the strong co-contraction of the lower arm muscles during pitch-tracking and during the PT, which was also observed in the other lower arm muscles FC and EC (not shown); all indicating a strong grip for these conditions.

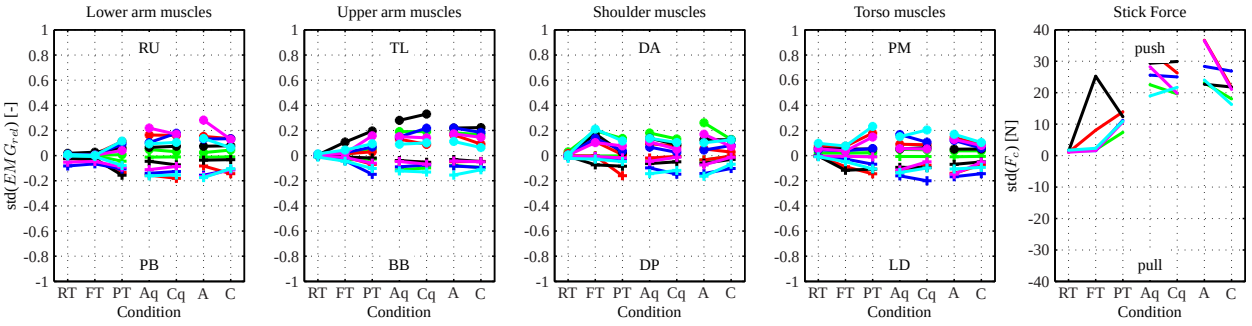

Figure 13. Standard deviation of the relative muscle activity EMG_{rel} for eight muscles of six pilots, measured over three runs.

Similar results can be observed in Figure Figure 12, which illustrates how much variability in muscle activity was present around the mean contraction level. Fluctuations are in the order of 20$\%$ of $EMGrel$, and are highest during all pitch control tasks and the position task.

V.C. Performance Parameters

Figure 14 shows the mean and 95% confidence intervals of the root-mean-square of the visual tracking error e, the stick deflection u and the stick contact force F_c.

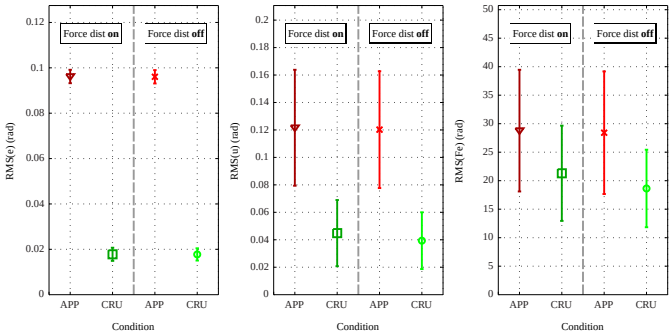

a) RMS(e) **b) RMS(u)** **c) RMS(F_c)**

Figure 14. Errorbar plots of the mean and 95% confidence intervals of the performance parameters.

The results show very significant differences in the means and variances of the RMS(e) and RMS(u) of the approach and cruise configurations. Smaller differences can be observed for the RMS(F_c).

No significant differences in the mean and variances were found between the conditions in which the force disturbance forcing function f_q was enabled and omitted. This supports the hypothesis that the force disturbance forcing function does not affect the control behavior.

V.D. Control Behavior Frequency Response Functions

Figures 15 and 16 show the identified frequency response functions of the visual (H_{p_e}) and the vestibular (H_{p_θ}) response. The crosses indicate the response at the elevator disturbance forcing function frequencies, the circles denote the response at the target frequencies. The response has been averaged over all pilots, and the errorbars represent the standard deviation. The solid lines show the fitted visual and vestibular models, again averaged over all the pilots. Figure 15 contains the results for the approach and cruise conditions in the presence of the force disturbance forcing function (f_q), while the results in Figure 16 were obtained without a force disturbance forcing function.

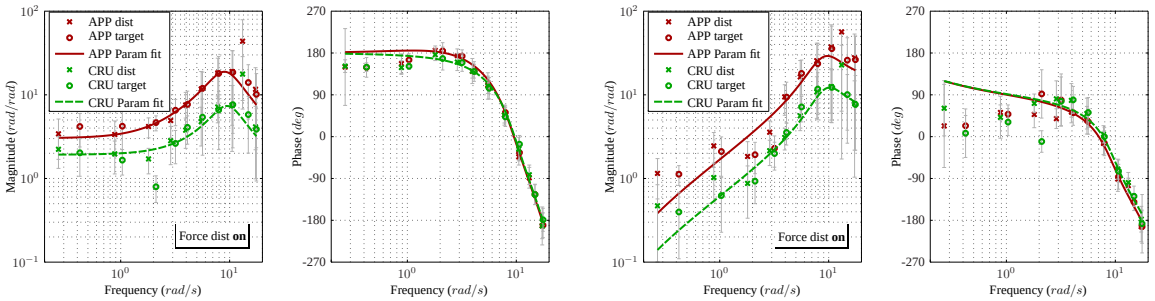

a) H_{p_e} **b)** H_{p_θ}

Figure 15. Pilot frequency response functions, identified in the presence of the force disturbance forcing function (f_q).

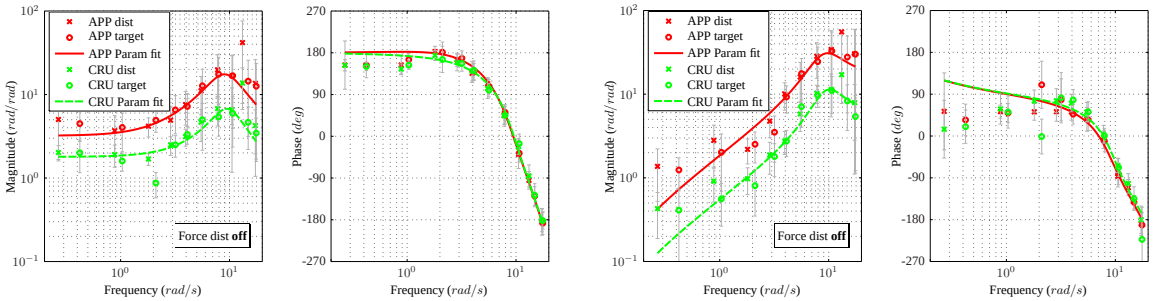

a) H_{p_e} **b)** H_{p_θ}

Figure 16. Pilot frequency response functions, identified without the force disturbance forcing function (f_q).

Both H_{p_e} and H_{p_θ} show the expected control behavior. H_{p_e} consists of a visual gain, transitioning into an differentiator around the short-period frequency of the aircraft pitch transfer function. This transition appears to occur at a slightly lower frequency for the approach condition. H_{p_θ} behaves as a differentiator, providing pitch rate information. The neuromuscular break frequency is present around 10 rad/s. Besides the lead time constant, the only significant difference between the approach and cruise conditions appears to be the visual and vestibular gains.

More important, no significant differences can be observed between 15 and 16, which means that the presence of the force disturbance forcing function f_q did not affect the visual and vestibular frequency response functions.

V.E. Control Behavior Parameters

The mean and standard deviation of the eight parameters in the visual and vestibular models are shown in Figure 17, both for the conditions with and without the presence of the force disturbance forcing function f_q.

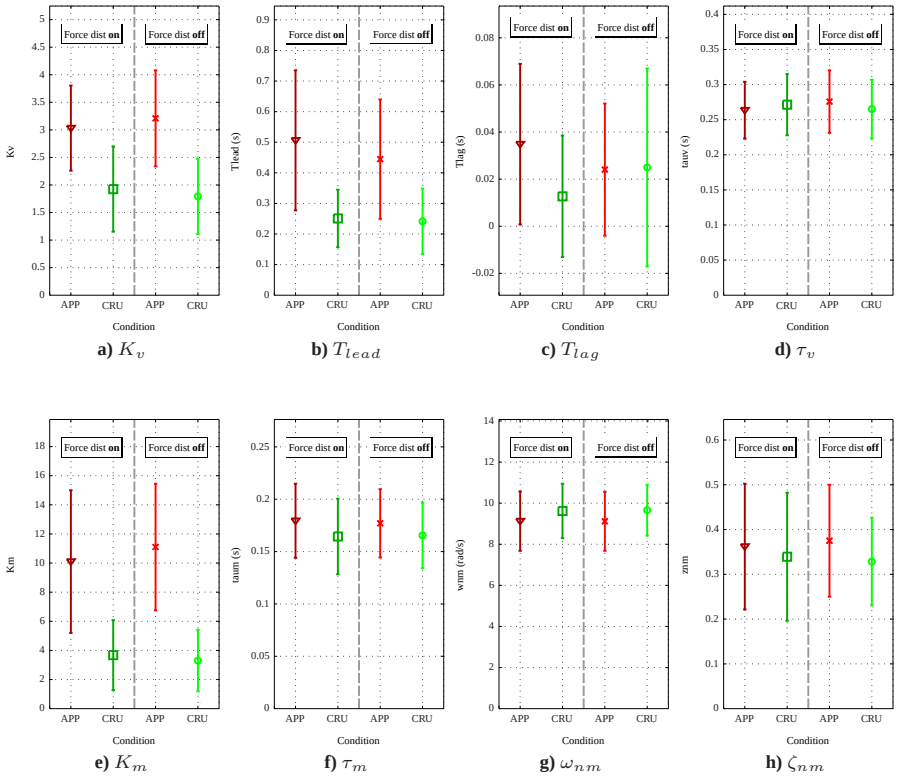

a) K_v **b)** T_{lead} **c)** T_{lag} **d)** τ_v

e) K_m **f)** τ_m **g)** ω_{nm} **h)** ζ_{nm}

Figure 17. Errorbar plots of the mean and 95% confidence intervals of the estimated model parameters.

It can be observed that no significant difference is observed between the conditions with and those without the presence of the force disturbance forcing function.

VI. Discussion

VI.A. Neuromuscular Admittance

The resulting identified admittance of the cruise and approach conditions raises two questions. Why does the admittance resembles the admittance of a position task? And secondly, what is causing the difference between the admittance in the cruise and approach conditions?

The admittance of the position, relax and force tasks agrees with values found in literature. This provides confidence in the measurement setup and the applicability of the methods to the identification of the admittance in the cruise and approach conditions. The standard deviation of the admittance in the cruise and approach conditions also is within an acceptable range. For this reason the identified admittance appears to be trustworthy.

Two possible causes for the low admittance are assumed. First, the pilot might have a poor internal representation of the vehicle and/or control inceptor dynamics, and will decrease his admittance to anticipate force disturbances, either external or internal (motor noise). A possible external source of force disturbances might be the simulator's linear and angular accelerations acting on the pilot's arm, resulting in biodynamic feedthrough.

A second cause of the low admittance might be the consequence of the difficulty of the task. The visual tracking task had a rather high task bandwidth (around 1 rad/s) and provoked a high-frequency control behavior. Participants might have contracted their muscles, thereby increasing their stiffness, to acquire a better precision or a more direct response, much like pretension. However, literature does not provide evidence to support this.

The fact that the admittance is smaller in the cruise condition than in the approach condition indicates that during cruise conditions there is either more co-contraction, more reflexive activity or more passive visco-elasticity (due to smaller stick deviation amplitudes). From the EMG measurements we know that the amount of co-contraction is fairly similar in both conditions, leaving reflexive activity and passive visco-elasticity (the amplitude effect) as possible causes. A parameter fit of the neuromuscular feedback system is required to determine whether the differences in admittance can be attributed to reflexive activity.

VI.B. EMG measurements

A very interesting finding from the EMG measurements were the high levels of co-contraction seen during all pitch tracking tasks. In some cases the co-contraction even exceeded those measured during the position task. Based on the results with other vehicle dynamics, hardly any co-contraction is expected when the vehicle dynamics are well known, since providing co-contraction is not energy-efficient and tiring. And even when the internal representation is poor, reflexive feedback is a more efficient way to respond to external force disturbances. As mentioned before, the co-contraction might be a result of the high-frequency task bandwidth and is a way to acquire a better precision or a more direct response, much like pretension. In order to investigate this, a new experiment should be performed in which a low-frequency task is executed, such as flying a normal approach.

VII. Conclusions

Under the experimental conditions studies, the following conclusions can be drawn:

- The variations of the control inceptor settings had a significant effect on the neuromuscular admittance, and showed that the stiffer cruise setting resulted in a lower admittance. A numbr of causes, such as different levels of co-contraction, reflexive feedback activity or amplitude effects, could have caused these effects. We were able to exclude variations in co-contraction as a cause due to the measurement of the muscle activity, which did not significantly differ between the conditions. In order to distinguishing between reflexive feedback activity or amplitude effects, the neuromuscular feedback model needs to be fitted to the measured admittance.

- The measured relative EMG signals revealed that the pitch control tracking tasks required very significant amounts of co-contraction. In some cases the levels of co-contraction during the tracking tasks even exceeded the co-contraction during the (postural) position task. This is very remarkable due to its energy inefficiency. The exact reason for the high co-contraction levels is not known, although a number of causes could be assumed.

- The variations of the control inceptor settings were not found to have a significant effect on the lumped neuromuscular parameters, the break frequency ω_{nm} and the damping ratio ζ_{nm}. This was in agreement with other studies.

- The applied force disturbance forcing function did not significantly affect the visual and vestibular control behavior exerted during the pitch control task. Neither the identified frequency response functions nor the fitted model parameters K_v, T_{lead}, T_{lag}, τ_v, K_m, tau_m, ω_{nm} or ζ_{nm} were significantly changed due to the introduction of the force disturbance function. In addition, also the mean and standard deviation of the measured muscle activity remained unaffected. For this reason it can be concluded that the method to measure neuromuscular admittance can be used without affecting the ontrol behavior.

References

[1]Belyavin, A., Woodward, A., Nguyen, D., Robel, G., and Woolworth, J., "Development of a Novel Model of Pilot Control Behavior in Balked Landings," *Proceedings of the AIAA Modeling and Simulation Technologies Conference and Exhibit, 15-18 August 2005, San Francisco, California*, American Institute of Aeronautics and Astronautics, August 2005, AIAA-2005-5878.

[2]Hosman, R. J. A. W., Schuring, J., and Van der Geest, P., "Pilot Model Development for the Manual Balked Landing Maneuvre," *Proceedings of the AIAA Modeling and Simulation Technologies Conference and Exhibit, 15-18 August 2005, San Francisco, California*, American Institute of Aeronautics and Astronautics, 2005, AIAA-2005-5884.

[3]Hosman, R. J. A. W., Schuring, J., Van der Geest, P., Belyavin, A., Robel, G., Towler, J. M., and Hörmann, H. J., "The Pilot Model Balked Landing Simulation Project: A Government, Industry and National Research Cooperation," *Proceedings of the Royal Aeronautical Society Conference: Civil and Military Simulator Qualification, London, November 9-10, 2005*, Royal Aeronautical Society, November 2005.

[4]Hosman, R. J. A. W., *Pilot's Perception and Control of Aircraft Motions*, Ph.D. thesis, Delft University of Technology, Faculty of Aerospace Engineering, 1996.

[5]McRuer, D. T., Graham, D., Krendel, E. S., and Reisener Jr., W., "Human Pilot Dynamics in Compensatory Systems. Theory, Models and Experiments with Controlled Element and Forcing Function Variations," AFFDL-TR 65-15, Wright-Patterson AFB(OH): Air Force Flight Dynamics Laboratory, August 1965.

[6]Hess, R. A., "Unified Theory for Aircraft Handling Qualities and Adverse Aircraft-Pilot Coupling," *Journal of Guidance, Control and Dynamics*, Vol. 20, No. 6, Nov.-Dec. 1997, pp. 1141–1148.

[7]Hall, G. W. and Smith, R. E., "Flight Investigation of Fighter Side-Stick Force-Deflection Characteristics," Tech. Rep. AFFDL-TR-75-39, Air Force Flight Dynamics Laboratory, May 1975.

[8]Diedrichsen, J., Shadmehr, R., and Ivry, R. B., "The coordination of movement : optimal feedback control and beyond," *Trends in Cognitive Sciences*, Vol. 14, No. December, 2009, pp. 31–39.

[9]Van der Helm, F. C. T., Schouten, A. C., De Vlugt, E., and Brouwn, G. G., "Identification of Intrinsic and Reflexive Components of Human Arm Dynamics During Postural Control," *Journal of Neuroscience Methods*, , No. 119, 2002, pp. 1–14.

[10]Abbink, D. A., *Neuromuscular Analysis of Haptic Gas Pedal Feedback during Car Following*, Ph.D. thesis, Delft University of Technology, Faculty of Mechanical Engineering, Dec. 2006.

[11]Damveld, H. J., Abbink, D. A., Mulder, M., Mulder, M., van Paassen, M. M., van der Helm, F. C. T., and Hosman, R. J. A. W., "Measuring the Contribution of the Neuromuscular System During a Pitch Control Task," *Proceedings of the AIAA Modeling and Simulation Technologies Conference, Chicago, Illinois, Aug. 10-13, 2009*, No. AIAA-2009-5824, American Institute of Aeronautics and Astronautics, Aug. 2009.

[12]Duque, J., Masset, D., and Malchaire, J., "Evaluation of handgrip force from EMG measurements," *Applied Ergonomics*, Vol. 26, No. 1, Feb. 1995, pp. 61–66.

[13]Venrooij, J., Mulder, M., van Paassen, M. M., Mulder, M., and Abbink, D. A., "Relating biodynamic feedthrough to neuromuscular admittance," *Proceedings of IEEE SMC Conference, San Antonia, USA*, October 2009.

[14]Goodrich, K. H., Schutte, P. C., and Williams, R. A., "Piloted Evaluation of the H-Mode, a Variable Autonomy Control System, in Motion-Based Simulation," *Proceedings of the AIAA Atmospheric Flight Mechanics Conference and Exhibit, Honolulu, Hawaii, Aug. 18-21, 2008*, No. AIAA-2008-6554, American Institute of Aeronautics and Astronautics, Aug. 2008.

[15]Doemges, F. and Rack, P. M. H., "Changes in the Stretch Reflex of the Human First Dorsal Interosseous Muscle During Different Tasks," *Journal of Physiology*, Vol. 447, Februari 1992, pp. 563–573.

[16]Doemges, F. and Rack, P. M. H., "Task-dependent Changes in the Response of the Human Wrist Joint to Mechanical Disturbance," *Journal of Physiology*, Vol. 447, Februari 1992, pp. 575–585.

[17]Kurtzer, I., DiZio, P., and Lackner, J., "Task-dependent Motor Learning," *Experimental Brain Research*, Vol. 153, No. 1, November 2003, pp. 128–132.

[18]Jaeger, R. J., Gottlieb, G. L., Agarwal, G. C., and Tahmoush, A. J., "Afferent Contributions to Stretch-evoked Myoelectric Responses," *Journal of Neurophysiology*, Vol. 48, No. 2, 1982, pp. 403–418.

[19]Stein, R. B. and Kearney, R. E., "Nonlinear Behavior of Muscle Reflexes at the Human Ankle Joint," *Journal of Neurophysiology*, Vol. 73, No. 1, 1995, pp. 65–72.

[20]Cathers, I., D'Dwyer, N., and Neilson, P., "Dependance of Stretch Reflexes on Amplitude and Bandwidth of Stretch in Human Wrist Muscle," *Experimental Brain Research*, Vol. 129, No. 2, November 1999, pp. 278–287.

[21]De Vlugt, E., Schouten, A. C., and Van der Helm, F. C. T., "Adaptation of Reflexive Feedback During Arm Posture to Different Environments," *Biological Cybernetics*, Vol. 87, No. 1, July 2002, pp. 10–26.

[22]Abbink, D. A., Van der Helm, F. C. T., and R., B. E., "Admittance Measurements of the foot during 'Maintain Position' and 'Relax' Tasks on a Gas Pedal," *Proceedings of the IEEE Conference on Systems, Man and Cybernetics*, October 2004.

[23] Abbink, D. A., "Task instruction: the largest influence on Human Operator Control Dynamics," *Proceedings of World Haptics 2007, Tsukuba, Japan, 22-24 March 2007*, March 2007, pp. 206–211.

[24] Lasschuit, J., Lam, T., Mulder, M., van Paassen, M. M., and Abbink, D., "Measuring and Modeling Neuromuscular System Dynamics for Haptic Interface Design," *AIAA Modeling and Simulation Technologies Conference and Exhibit, 18 - 21 August 2008, Honolulu, Hawaii*, August 2008.

[25] Abbink, D. A., Mugge, W., Schouten, A. C., DeWald, J., and van der Helm, F. C. T., "A rigorous model of reflex function indicates that position and force feedback are flexibly tuned to position and force tasks," *Experimental Brain Research*, 2009, conditionally accepted 2009.

[26] Schouten, A. C., De Vlugt, E., Van Hilten, J. J. B., and Van der Helm, F. C. T., "Quantifying Proprioceptive Reflexes During Position Control of the Human Arm," *IEEE Transactions on Biomedical Engineering*, Vol. 55, No. 1, January 2008, pp. 311–321.

[27] Mitchell, D. G., Aponso, B. L., and Klyde, D. H., "Effects of Cockpit Lateral Stick Characteristics on Handling Qualities and Pilot Dynamics," Tech. Rep. NASA-CR-4443, National Aeronautics and Space Administration, June 1992.

[28] Mugge, W., Abbink, D. A., and Van der Helm, F. C. T., "Reduced Power Method: how to evoke low-frequent behaviour while estimating high-bandwidth admittance," *Proceedings of the International Conference on Robotics and Rehabilitation, Noordwijk, the Netherlands, June 2007*, June 2007.

[29] Hosman, R. J. A. W. and van der Vaart, J. C., "Vestibular Models and Thresholds of Motion Perception. Results of Tests in a Flight Simulator," Report LR-265, Delft University of Technology, Faculty of Aerospace Engineering, 1978.

[30] Mulder, M., *Cybernetics of Tunnel-in-the-Sky Displays*, Ph.D. thesis, Delft University of Technology, Faculty of Aerospace Engineering, 1999.

[31] Nieuwenhuizen, F. M. and Zaal, P. M. T., "Modeling Human Multichannel Perception and Control Using Linear Time-Invariant Models," *Journal of Guidance, Control, and Dynamics*, Vol. 31, No. 4, July-August 2008, pp. 999–1013.

[32] Van Lunteren, A., *Identification of Human Operator Describing Function Models with One or Two Inputs in Closed Loop Systems*, Ph.D. thesis, Delft University of Technology, Faculty of Mechanical Engineering, 1979.

[33] Ljung, L., *System Identification: Theory for the user*, Prentice-Hall, Inc., 1987.

[34] Van Paassen, M. M., Stroosma, O., and Delatour, J., "DUECA - Data-driven Activation in Distributed Realtime Computation," *Proceedings of the AIAA Modeling and Simulation Technologies Conference, Denver, CO, Aug. 14-17, 2000*, No. AIAA-2000-4503, American Institute of Aeronautics and Astronautics, August 2000.

[35] Smaili, H., Breeman, J., Lombaerts, T., and Stroosma, O., "A Benchmark for Fault Tolerant Flight Control Evaluation," *Proceedings of the 7th IFAC Symposium on Fault Detection, Supervision and Safety of Technical Processes, June 30 - July 3, 2009, Barcelona, Spain*, International Federation of Automatic Control, 2009.

[36] Reid, L. D. and Nahon, M., "Flight Simulation Motion-base Drive Algorithms: 1 - Developing and Testing the Equations," UTIAS Report 296, University of Toronto Institute for Aerospace Studies, 1985.

[37] Reid, L. D. and Nahon, M., "Flight Simulation Motion-base Drive Algorithms: Part 2 - Selecting the System Parameters," UTIAS Report 307, University of Toronto Institute for Aerospace Studies, 1986.

[38] Sinacori, J. B., "The Determination of Some Requirements for a Helicopter Flight Research Simulation Facility," NASA-CR 152066, National Aeronautics and Space Administration, September 1977.

[39] Schroeder, J. A., "Helicopter Flight Simulation Motion Platform Requirements," NASA-TP 1999-208766, National Aeronautics and Space Administration, July 1999.

[40] Damveld, H. J., *A Cybernetic Approach to Assess the Longitudinal Handling Qualities of Aeroelastic Aircraft*, Ph.D. thesis, Delft University of Technology, Faculty of Aerospace Engineering, May 2009.

[41] Damveld, H. J., Beerens, G. C., van Paassen, M. M., and Mulder, M., "Design of Forcing Functions for the Identification of Human Control Behavior," *Journal of Guidance, Control, and Dynamics*, Vol. 33, No. 4, July 2010, pp. 1064–1081.